optica

Optical imaging through dynamic turbid media using the Fourier-domain shower-curtain effect

EITAN EDREI AND GIULIANO SCARCELLI*

Fischell Department of Bioengineering, University of Maryland, College Park, Maryland 20742, USA
**Corresponding author: scarc@umd.edu*

Received 21 October 2015; revised 13 December 2015; accepted 13 December 2015 (Doc. ID 252407); published 13 January 2016

Several phenomena have been recently exploited to circumvent scattering and have succeeded in imaging or focusing light through turbid layers. However, the requirement for the turbid medium to be steady during the imaging process remains a fundamental limitation of these methods. Here, we introduce an optical imaging modality that overcomes this challenge by taking advantage of the so-called shower-curtain effect, which is adapted to the spatial-frequency domain via speckle correlography. We present high-resolution imaging of objects hidden behind millimeter-thick tissue or dense lens cataracts. We demonstrate our imaging technique to be insensitive to rapid medium movements (>5 m/s) beyond any biologically relevant motion. Furthermore, we show this method can be extended to several contrast mechanisms and imaging configurations.

OCIS codes: (110.0113) Imaging through turbid media; (290.4210) Multiple scattering; (030.6140) Speckle.

http://dx.doi.org/10.1364/OPTICA.3.000071

All-optical imaging through scattering turbid media is among the biggest challenges in optics and has important applications in many biomedical and engineering fields [1]. Pioneering work toward this goal has been recently demonstrated using phenomena such as the memory effect [2–4], phase conjugation [5], and the scattering matrix inversion [6–8]. However, a fundamental issue toward practical applications remains the requirement that the turbid media should be stationary, as slight movements dramatically degrade the image quality [3,9]. Recent studies have shown significant progress toward this goal by demonstrating rapid focusing through dynamic scattering layers [10,11]. Here, we present an all-optical method based on the so-called "shower-curtain" effect, which enables imaging behind millimeter-thick tissues and is fundamentally insensitive to turbid medium motions.

The shower-curtain effect is a familiar phenomenon, routinely observed in our everyday life: an object placed behind a scattering layer appears blurred [Figs. 1(a) and 1(b)], but if the object is attached to the scattering layer, it can be clearly resolved [Fig. 1(c)]. The shower-curtain effect is known to represent an obstacle to high-quality imaging [12,13]. From an optics standpoint, the scattering layer behaves as a short-pass filter for spatial frequencies: as the distance between the object and the scattering layer increases, the frequency cutoff decreases, thus reducing the imaging resolution [14–16]. However, at short distances, the cutoff frequency is high enough that objects can be seen at high resolution even through a turbid medium of several scattering lengths (Fig. S1, Supplement 1). Interestingly, the spatial correlations between the front side and back side of the turbid medium that are exploited in the shower-curtain effect can be considered as the near-field counterpart of the spatial correlations exploited in memory effect protocols (Fig. S2, Supplement 1) [17]; however, working in an imaging configuration, the near-field correlations exploited in the shower-curtain effect can be made robust against turbid medium motions (Fig. S3, Supplement 1). The optical system we developed takes advantage of the shower-curtain effect properties and generalizes them to achieve high-resolution imaging of objects placed at a nearly arbitrary distance behind the scattering medium. The imaging procedure is based on retrieving the object's Fourier transform from the turbid medium (used as the shower curtain) through a correlography technique based on speckle illumination.

Imaging correlography [18–20], which was developed in the 1980s, uses similar principles as speckle interferometry [21,22]. A coherent beam is diffused by a scattering object, giving rise to a speckled object field $f_n(x,y)$, where the subscript n refers to a specific speckle configuration emerging from the object. After propagation to the far field, a two-dimensional Fourier transform, $|\tilde{F}[f_n(x,y)]|^2$ can be observed. By the Wiener–Khinchin theorem, the Fourier transform of this pattern is related to the autocorrelation of the speckled object: $\tilde{F}^{-1}[|\tilde{F}[f_n(x,y)]|^2] = f_n(x,y) * f_n(x,y)$. Averaging over many independent realizations of processed speckle patterns, the autocorrelation of the original object can be obtained (see Supplement 1) [18–20]. From the autocorrelation, a phase retrieval algorithm can be applied to image the object [23,24]. Traditional imaging correlography techniques are not suitable for imaging close objects behind highly scattering media. Here, we overcome these issues through the aforementioned shower-curtain effect and with speckle illumination. By illuminating the object with a speckle pattern rather than a coherent beam, we extend the correlography technique to transmitting or other nonscattering objects. More importantly, we show that the correlography principles can be effectively applied

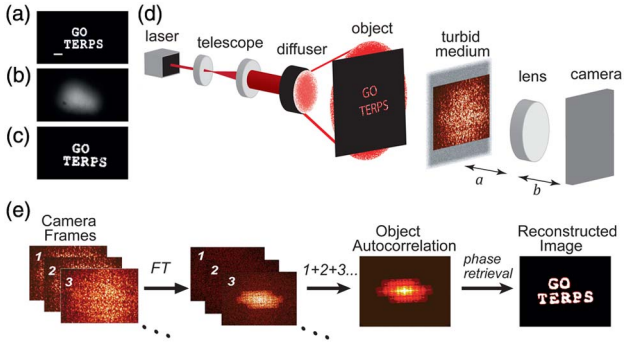

Fig. 1. Shower-curtain phenomenon, data acquisition, processing, and results. (a) Object mask imaged in free space. Scale bar, 200 μm. (b) The object placed 5 mm behind a ground glass diffuser appears blurred. (c) The object placed very close to the ground glass diffuser can be seen clearly. (d) Experimental setup: an expanded laser beam is diffused by a first diffuser; the scattered light passes through the object and generates a complex pattern on a turbid medium. The plane of the turbid medium is imaged onto the camera with a lens of focal length $f(1/a + 1/b = 1/f)$. (e) Data processing and experimental results: the acquisition procedure is repeated many times while the first diffuser is shifted. For each frame, we performed a Fourier transform, DC filtering, and averaging to obtain the autocorrelation of the object. From the autocorrelation, we retrieved the object with a phase retrieval algorithm.

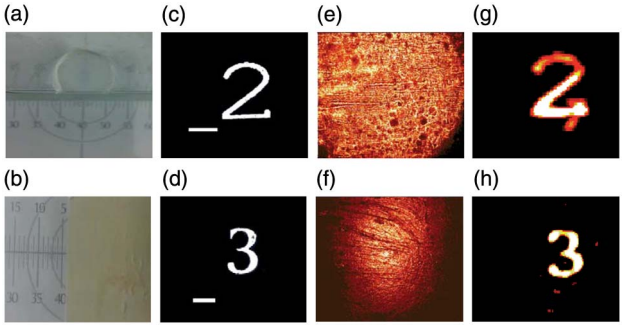

Fig. 2. Imaging through biological turbid media. (a) and (b) Photograph of a ruler placed 0.5 in hidden behind a cataract and an 0.8-mm-thick chicken breast tissue. (c) Object mask used for imaging through cataract. Scale bar, 200 μm. (d) Object mask used for imaging through the chicken tissue. Scale bar, 100 μm. (e) and (f) Average of the recorded images as seen through the cataract and the tissue (distances 80 and 100 mm, respectively). (g) and (h) The reconstructed images as obtained after correlography analysis.

in the near field. While the far-field condition is usually known as $z > 2D^2/\lambda$ (D, size of the object; λ, wavelength), by tuning the spatial coherence of the illumination beam, as one can do with speckle illumination, the "far-field" condition can be written as $z > 2DR_c/\lambda$, where R_c is the correlation radius of the speckle pattern (see Supplement 1) [25]. We experimentally verified this property by illuminating a double-slit aperture (width 150 μm, separation 1 mm) with a coherent beam and with a speckle pattern. Placing the camera in the near field (50 mm), we observed the double-slit Fresnel diffraction pattern as expected [Figs. S4(a) and S4(b),Supplement 1]; however, by performing our correlography-based reconstruction, we obtained the Fourier transform of the double slit as if we were working under the Fraunhofer "far-field" diffraction condition [Figs. S4(c) and S4(d), Supplement 1]. Using this property, in practice, for objects with sizes ranging between 100 μm and 1 mm, the Fourier transform can traditionally only be recorded at distances as high as tens of centimeters; instead, we can reduce this distance requirement by one to two orders of magnitude by tuning the illuminating speckle size between 1 and 10 μm. This makes our technology compatible with biomedical applications such as retinal imaging behind cataracts or imaging of the back of the ear behind the tympanic membrane.

Our experimental setup, processing procedure, and exemplary results are shown in Fig. 1. We employed an He–Ne laser beam at 632 nm; after expanding the beam, we used a ground glass diffuser to generate the speckle pattern that illuminates the aperture mask (object). Light transmitted through the object hit a second diffuser, which acted as the turbid medium of interest. Through the shower-curtain effect, the light pattern projected on the front side of the turbid medium can be observed on the back side of the turbid medium. To record such a pattern, one can either place a camera in the plane of the turbid medium, or, as we did, image the plane of the turbid medium onto a camera with a lens. After recording 3000 frames while shifting the first diffuser [Fig. S5(a), Supplement 1], we Fourier transformed, processed, and summed each frame to yield the autocorrelation of the object. At last, we reconstructed the original object from the autocorrelation using Fienup phase retrieval algorithm [Fig. 1(e)].

To present our imaging performances through biological tissues, we used a dense nuclear cataract from *ex vivo* rabbit eyes and a 0.8-mm-thick chicken breast tissue. Both these turbid media are visually opaque, i.e., standard systems cannot image objects hidden behind them [Figs. 2(a) and 2(b)]. For our experiment, we used objects printed on a photolithography mask, with the smallest features ∼10 μm [Figs. 2(c) and 2(d)]. We illuminated the objects with a speckle pattern, as previously described, and recorded the transmitted light at the back surface of the turbid medium. The conventional imaging system yielded no information about the objects [Figs. 2(e) and 2(f)]; instead, our reconstruction process accurately retrieved the shape of the original objects [Figs. 2(g) and 2(h)].

A key feature of the shower-curtain phenomenon is that any phase aberration introduced in the plane of the turbid medium does not affect the intensity pattern recorded if that plane is imaged onto a camera. Thus, in our scenario, the turbid medium can be effectively thought of as a screen where images or other light patterns are projected and recorded. As a result, the turbid medium is not required to be stable during the imaging process; in fact, operating in an imaging configuration, dynamic scattering processes occurring at the turbid medium plane do not contribute to the degradation of the point-to-point correspondence of the imaging system. To vividly demonstrate this intriguing property, we used a ground glass as a turbid medium, and we rapidly rotated it (37 revs/s) using a commercial fan [Fig. 3(a)], yielding greater than 5 m/s linear speed at the pattern location. We used the same object aperture as in the static case [Fig. 3(b)]. As expected, neither the single shot of the camera [Fig. 3(c)] nor the average of all recorded frames [Fig. 3(d)] seemed to provide useful information about the object; however, by adding the processed Fourier transforms of all images and applying the phase retrieval algorithm, we could reconstruct a clear image of the object [Fig. 3(e)]. In our method, the quality of the reconstructed image through a highly dynamic turbid medium is as good as the one obtained with static

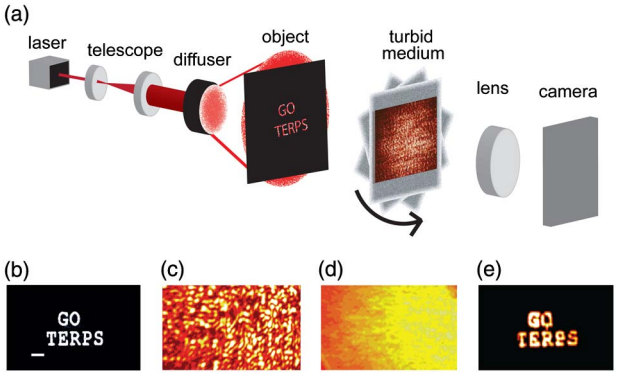

Fig. 3. Imaging through dynamic turbid media. (a) Experimental setup: an expanded laser beam is scattered by a ground glass diffuser and the resulting speckle pattern illuminates an object. The light transmitted through the object propagates 190 mm and goes through a rapidly rotating ground glass. We used a camera to record the light pattern on the rotating ground glass. (b) Object. Scale bar, 200 μm. (c) Representative single shot as recorded by the camera. (d) Average of 3000 camera frames of different speckle realizations. (e) Reconstructed image.

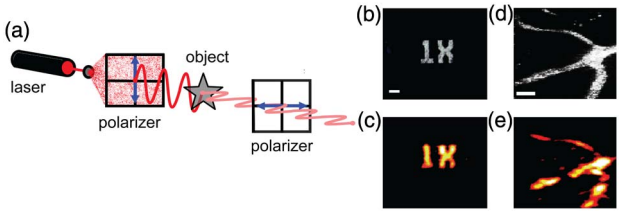

Fig. 5. Different contrast mechanisms. (a) Schematic principle of the experimental setup. (b) and (c) We placed an object made of fixed corneal tissue between two cross polarizers so that only light that changed polarization went through. The distance between the object and the turbid medium here was 55 mm. (b) Object aperture imaged in free space. Scale bar, 250 μm. (c) Reconstructed image. (d) and (e) Between two cross polarizers, we placed a dried retinal tissue sample so that only light scattered by tissue features went through. The distance between the object and the turbid medium here was 140 mm. (d) Retinal tissue object imaged in free space in a cross polarized configuration. Scale bar, 250 μm. (e) Reconstructed image through turbid medium.

turbid medium [Fig. S3(a), Supplement 1]. The speckle decorrelation time introduced by the turbid medium in this scenario is shorter than 1 μs [Fig. S5(b), Supplement 1], which is several orders of magnitude faster than the camera acquisition time. This would dramatically degrade the spatial correlations used in memory-effect-based protocols, as shown in Fig. S3(b), Supplement 1, thus confirming the great improvements offered by our protocol in terms of motions of the scattering medium.

Beyond transmission configurations, we demonstrated our imaging protocol in the "look around the corner" geometry. We used a similar setup to Fig. 1, but we collected the light scattered off the turbid medium [Fig. 4(a)]. High-quality image reconstructions were obtained also in this configuration [Figs. 4(b) and 4(c)].

Furthermore, our imaging protocol can be extended to contrast mechanisms other than transmission. As a proof-of-principle demonstration, we used the object birefringence as the imaging contrast [Fig. 5(a)]. To make a birefringent object, we surgically extracted and fixed a bovine cornea; we stained it with picrosirius red (PSR) and attached it to a USAF chart [Fig. 5(b)]. The PSR staining of the collagen-rich tissue sample changed the polarization of the incoming light; therefore, placing two crossed polarizers before and after the object, the recorded pattern was only due to the birefringence contrast, while the light transmitted with no polarization change was effectively suppressed (18 fold). Our imaging protocol was clearly able to reconstruct the shape of the birefringent regions of the object [Fig. 5(c)]. This result shows that our protocol can be generalized to dark-field microscopy configurations, where a positive contrast is obtained from the object on a dark background. We used the same cross-polarized setup to image a bovine retinal tissue sample through a ground glass diffuser. Only light that was scattered by the different features in the tissue was collected by the imaging system, as shown by directly imaging the tissue with standard polarized microscopy [Fig. 5(d)]. Also in this case, our reconstruction process was able to retrieve the object shape through the turbid medium [Fig. 5(e)]. Together, Figs. 4 and 5 demonstrate that our imaging protocol could be extended to *epi* detection configurations for biomedical applications where objects can only be accessed from one side.

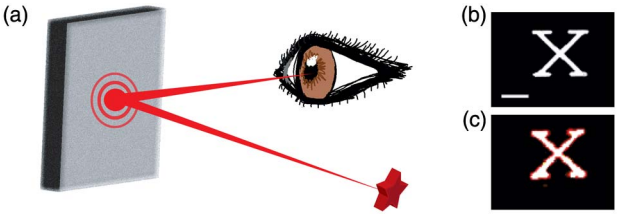

Fig. 4. Imaging around the corner. (a) In the reflection configuration, we recorded the light scattered off the turbid medium. For these experiments, as the turbid medium, we used white paper located 150 mm from the object. (b) Object. Scale bar, 200 μm. (c) Reconstructed image.

At a fundamental level, the spatial correlations exploited by the shower-curtain phenomenon are governed by the same principles as the ones used in the memory effect [17,26,27]. The angular range of the memory effect can be thought of as the maximum numerical aperture through which an object can be observed, and thus provides an upper limit on the spatial frequency cutoff of the shower curtain. We quantitatively demonstrated this correspondence in Fig. S2 of Supplement 1. Hence, in static conditions, image protocols that use the shower-curtain effect will be able to reconstruct objects through the same scattering layers as the pioneering work by Bertolotti *et al.* [2] and Katz *et al.* [3], with equivalent limitations on resolution and field of view. In particular, our protocol uses coherent processing to exploit the shower-curtain effect in the Fourier domain, i.e., the features we measure through the scattering layer are the spatial frequencies of the object rather than the object features. Therefore, the scattering medium primarily degrades the field of view (FOV) rather than the resolution of the imaging system. The maximal FOV for imaging is found to be $\theta_{\max} < \lambda/\pi R_t$, with R_t being the smallest resolvable feature on the turbid medium plane. For a ground glass diffuser, we measured $R_t < 8$ μm, corresponding to FOV ~1.5°; for the 0.8 mm chicken tissue, we measured $R_t < 20$ μm, corresponding to FOV ~0.6°. The resolution of the system instead is given by how many Fourier components can be recorded at a high signal-to-noise ratio. Thus, the lens that images the turbid medium plane onto the camera has to provide enough resolution to distinguish R_t and enough field of view to capture the full

Fourier spectrum of the object. For a ground glass turbid medium located 35 mm from the object, we obtained a 3 μm resolution corresponding to an effective NA of 0.1 compared to the geometrical 0.16 NA of the system. Diffraction-limited resolution can be obtained by optimizing the pixel size, speed, and sensitivity of the camera sensor. Working in the Fourier domain may be advantageous because by enlarging the distance between object and scattering layer, thicker media can be handled; we demonstrated this property by imaging an object with 10-μm-sized features behind a 3.3-mm-thick piece of chicken breast tissue (Fig. S6, Supplement 1). However, the ultimate thickness of the scattering medium is limited, as the light-diffusion delay spread within the turbid medium should not exceed the temporal coherence set by the first diffuser [3].

In dynamic conditions where the turbid medium is moving and light correlations are degraded, our protocol is markedly different from memory-effect protocols. Three peculiar features (i.e., near-field correlations through the shower curtain, coherent formation of the object Fourier transform, and direct readout of the object Fourier transform in an imaging configuration) contribute to make our protocol nearly insensitive to the motions of the scattering medium. We have shown that in scenarios where the speckle decorrelation time introduced by the turbid medium is several orders of magnitude faster than the detector response time, the spatial correlations of the speckle patterns are much degraded, while our protocol is not affected (Fig. S3, Supplement 1). Being based on the Fourier transform retrieval, however, our method is inherently a coherent technique. Therefore, unlike previous incoherent reconstructions, broadband contrast mechanisms such as fluorescence are difficult to use. This also represents the practical limit on the motion of turbid media that can be handled. To retrieve high-quality Fourier transforms, the single-frame acquisition time should be faster than the speckle decorrelation time of the first diffuser, which in epi-detection configurations may also be a moving biological tissue. With our low-cost camera, we operated in the order of a 10 ms acquisition time, which would already allow imaging without artifacts caused by breathing, saccadic movements or heartbeats. It is straightforward to improve this performance and achieve sub-millisecond acquisition times using a more sensitive camera.

In summary, we demonstrated a speckle correlography protocol based on the shower-curtain effect adapted to the Fourier domain. This enabled imaging through millimeter-thick tissues, which is insensitive to turbid medium motions. Using light power levels safe for *in vivo* tissue applications and low-cost optical components, we demonstrated imaging performances that are promising for biomedical applications, such as imaging the retina through a cataract or the back of the ear through the tympanic membrane.

Funding. Human Frontier Science Program (HFSP) (RGY0074/2013); Ministry of Science of Korea (IITP-2015-R0346-15-1007); National Institute of Biomedical Imaging and Bioengineering (NIBIB) (K25-EB015885); University of Maryland (UMD) (Tier 1 Award).

See Supplement 1 for supporting content.

REFERENCES

1. V. Ntziachristos, Nat. Methods **7**, 603 (2010).
2. J. Bertolotti, E. G. van Putten, C. Blum, A. Lagendijk, W. L. Vos, and A. P. Mosk, Nature **491**, 232 (2012).
3. O. Katz, P. Heidmann, M. Fink, and S. Gigan, Nat. Photonics **8**, 784 (2014).
4. X. Yang, Y. Pu, and D. Psaltis, Opt. Express **22**, 3405 (2014).
5. Z. Yaqoob, D. Psaltis, M. Feld, and C. Yang, Nat. Photonics **2**, 110 (2008).
6. Y. Choi, T. D. Yang, C. Fang-Yen, P. Kang, K. J. Lee, R. R. Dasari, M. S. Feld, and W. Choi, Phys. Rev. Lett. **107**, 023902 (2011).
7. O. Katz, E. Small, and Y. Silberberg, Nat. Photonics **6**, 549 (2012).
8. S. M. Popoff, G. Lerosey, R. Carminati, M. Fink, A. C. Boccara, and S. Gigan, Phys. Rev. Lett. **104**, 100601 (2010).
9. D. B. Conkey, A. M. Caravaca-Aguirre, and R. Piestun, Opt. Express **20**, 1733 (2012).
10. D. Wang, E. H. Zhou, J. Brake, H. Ruan, M. Jang, and C. Yang, Optica **2**, 728 (2015).
11. Y. Liu, P. Lai, C. Ma, X. Xu, A. A. Grabar, and L. V. Wang, Nat. Commun. **6**, 5904 (2015).
12. L. Thrane, H. T. Yura, and P. E. Andersen, J. Opt. Soc. Am. A **17**, 484 (2000).
13. S. Jaruwatanadilok, A. Ishimaru, and Y. Kuga, IEEE Trans. Geosci. Remote Sens. **41**, 1834 (2003).
14. Y. Kuga and A. Ishimaru, Appl. Opt. **25**, 4382 (1986).
15. I. Dror, A. Sandrov, and N. S. Kopeika, Appl. Opt. **37**, 6495 (1998).
16. V. V. Belov and B. D. Borisov, Proc. SPIE **4338**, 8 (2000).
17. I. Freund, Phys. A **168**, 49 (1990).
18. P. S. Idell, J. R. Fienup, and R. S. Goodman, Opt. Lett. **12**, 858 (1987).
19. P. S. Idell, J. D. Gonglewski, D. G. Voelz, and J. Knopp, Opt. Lett. **14**, 154 (1989).
20. D. G. Voelz, J. D. Gonglewski, and P. S. Idell, Appl. Opt. **30**, 3333 (1991).
21. A. Labeyrie, Astron. Astrophys. **6**, 85 (1970).
22. J. C. Dainty, *Laser Speckle and Related Phenomena*, Topics in Applied Physics (Springer-Verlag, 1975), Vol. **9**, p. 298.
23. J. R. Fienup, Opt. Lett. **3**, 27 (1978).
24. J. R. Fienup, Appl. Opt. **21**, 2758 (1982).
25. J. W. Goodman and R. L. Haupt, *Statistical Optics* (Wiley, 2015).
26. A. P. Mosk, A. Lagendijk, G. Lerosey, and M. Fink, Nat. Photonics **6**, 283 (2012).
27. B. Judkewitz, R. Horstmeyer, I. M. Vellekoop, I. N. Papadopoulos, and C. Yang, Nat. Phys. **11**, 684 (2015).